CONFORMAL TUNGSTEN DISULPHIDE SOLID LUBRICANT NANOCOMPOSITE COATINGS ON ROLLING ELEMENT BEARINGS

T. W. Scharf, B. P. Gorman, S. V. Prasad*, and M. T. Dugger*
The University of North Texas, Department of Materials Science and Engineering, Denton, TX 76203
**Sandia National Laboratories, Albuquerque, New Mexico 87185*

ABSTRACT

This paper describes the synthesis, structure, tribological, and torque behavior of nanocomposite (ZnF_2 in WS_2 matrix) solid lubricant coatings grown by atomic layer deposition (ALD) with application to fully assembled rolling element bearings. The coatings were grown by sequential exposures of WF_6 and H_2S gases with a diethyl zinc catalyst in a viscous flow reactor from 250 to 350ºC on fully assembled 440C stainless steel rolling element bearings and witness Au, Si and SiO_2 substrates. Coatings were studied by cross-sectional scanning and transmission electron microscopies and x-ray diffraction to determine the coating conformality and crystallinity. The coatings exhibited a hexagonal layered structure with predominant preferentially orientated (002) basal planes normal to the substrate. These basal planes when sheared imparted very low friction ($\mu \sim 0.008$) and wear rates ($\sim 2.4 \times 10^{-7}$ $mm^3/N \cdot m$) in a dry nitrogen testing environment. In addition, the coatings were conformally and uniformly deposited on fully assembled bearings in cartridges to study the rolling torque behavior in dry nitrogen and lab air during oscillatory contacts and after exposure to vibration. It was found the outer race, inner race and ball surfaces tested showed third body (transfer film) protection necessary to achieve low torque (~0.5 mN.m) in dry nitrogen. In contrast, testing in air showed almost total oxidation of WS_2 coatings and some areas with no WS_2. The ALD deposition of solid lubricants for miniature bearings is thus an attractive alternative to present lubrication methods since it offers the potential for reduced particulate contamination, more consistent run-in behavior due to more uniform lubricant distribution, and the ability to use relatively low cost, fully-assembled stainless steel bearings and batch processing to minimize lubrication process costs.

KEYWORDS: Tribological Materials/Tribology/Wear; Coatings/Films; Applications-Aerospace

1. INTRODUCTION

Transition metal dichalcogenides, such as tungsten disulphide (WS_2) and molybdenum disulfide (MoS_2), are well known for their solid lubricating behavior especially for aerospace applications [1-7]. Compared with MoS_2, WS_2 exhibits higher thermally stability [8] and provides a ~ 100ºC increase in maximum operating temperature [9,10]. In the WS_2 layered structure, a sheet of tungsten atoms is sandwiched between two hexagonally packed sulphur layers. The bonding within the S-W-S sandwich is covalent, while weak Van der Waals forces hold the sandwich together resulting in interlamellar mechanical weakness. Thus, under a shearing force the basal planes slide back and forth over one another by intracrystalline slip and transfer to the rubbing counterface. These mechanisms for imparting low friction have already been studied in the literature [1-4,11] and low friction coefficients are realized if there is a) the development of a transfer film on the counterface to accommodate interfacial sliding, b) reorientation of the (002) basal plane parallel to the sliding direction in the wear track, and c) the absence of contaminants such as oxygen, carbon, and water. Thus, low friction coefficients (0.01 to 0.05 depending upon normal load) of these coatings are only exhibited in either dry inert gas or in ultrahigh vacuum [11,12]. Friction coefficients of 0.03 to 0.05 have been reported in dry nitrogen for pulsed laser deposited WS_2 [10,13] and 0.02 to 0.06 for sputtered coatings [13]. Similarly, we have recently reported very low friction coefficients down to ~0.008 and low wear

factors ($2.4x10^{-7}$ $mm^3/N \cdot m$) for WS_2 coatings [14]. Conversely, when sliding in humid air, dangling or unsaturated bonds on the edge of basal planes react with moisture and oxygen in the environment forming WO_3 that has a high friction coefficient (> 0.15) and poor wear behavior [13].

Solid lubricant coatings are typically applied by physical vapor deposition (PVD) techniques, such as sputter deposition [1,5,15], pulsed laser ablation [10,13,16], burnishing/impingement, evaporation [6,17], or metal organic chemical vapor deposition (MOCVD) [18-21]. Several of these processes are line-of-sight, making it difficult to coat surfaces shadowed from the target, or uniformly coat sidewalls of three-dimensional or high aspect ratio structures. While the CVD techniques can coat shadowed surfaces, high temperatures are required for absorption and decomposition of chemical precursors on the surface, limiting its application. For applications such as stainless steel miniature rolling element bearings, where dimensions and separation tolerances are small and tempering of the steel is problematic, these line-of-sight and high temperature deposition techniques are inadequate.

Thus, an effective low temperature coating process must be able to transport material into these confined spaces and deposit a film of equal thickness, composition, and properties to that deposited on exposed parts of the device. The self-limiting nature of the atomic layer deposition (ALD) process is ideally suited to provide uniform and conformal coating of fully assembled miniature rolling element bearings. The ALD process is a surface reaction controlled variant of the CVD technique. It uses the sequential introduction of gaseous precursors and selective surface chemistry to achieve atomic scale controlled growth at reduced temperatures ranging from 100 to 400ºC [22-24]. Because of the self-limiting nature of ALD, the coatings have very uniform thickness even if the flux of vapor is distributed non-uniformly over the surface. This efficient transport of material into confined spaces at low pressure, and sequential introduction of reactants leads to excellent control of coating thickness and coverage of high aspect ratio structures [22-24]. Previously, our group determined the ALD WS_2 was effective in conformally and uniformly coating polycrystalline Si and electroplated Ni microelectromechanical systems (MEMS) structures [14]. Here we apply the same ALD process to coat shadowed and buried surfaces of rolling element bearings, where decreasing the size of mechanical assemblies motivates the use of miniature bearings.

Small electromechanical devices that employ rotary actuators, such as rotary solenoids, make use of miniature bearings (outer diameter < 1 cm) in order to provide high-precision rotary motion with minimal torque loss. Electromechanical devices for weapon security applications are required to operate consistently in a nitrogen atmosphere at temperatures from -55°C to 80°C, after assembly and testing in humid air, and after storage for up to 25 years without actuation. These applications also require the lubricant to survive low level vibration for decades during transportation of the devices, and high level vibration during rocket launch, without damage to the balls or races. Solid lubricants, such as MoS_2 and WS_2, are ideally suited to the requirements of such applications due to their consistent performance over a wide range of temperatures, low outgassing and migration rates, and low wear rates in vacuum or inert atmospheres. Hybrid bearings (ceramic balls such as Si_3N_4 in steel races), generally do not survive the vibration environments without damage to the steel races. Thin films of solid lubricants deposited by PVD techniques on bearing balls or races are difficult to control precisely on curved race surfaces, and excess lubricant worn from races during run-in leads to torque noise or sources of particulate contamination for sensitive electrical contacts. Coating of balls or races is also very costly due to being highly labor intensive, even for batch processing. Simple burnishing of solid lubricant powders into fully-assembled steel bearings is another potential approach, but torque noise and concerns for particulate contamination remain. Thus, there remains a need for solid lubricant materials and deposition methods that result in control of thickness to better than 0.1 micron on very complex, curved surfaces that may be deeply buried inside an assembled bearing, such as between retainers and balls, or balls and races. The ability to apply these materials to fully assembled steel bearings is also desirable, since relatively inexpensive steel bearings can be used. In this study, we evaluated ALD WS_2 solid lubricants on

miniature rolling element bearings, compared to sputter-deposited and impingement MoS_2 coatings. Bearing torque as a function of oscillatory cycles and vibration are determined, as well as the composition (energy dispersive x-ray spectroscopy) and microstructure (cross-sectional scanning and transmission electron microscopies) of the coatings before and after torque measurements, to determine changes in structure that occur during use of the coatings.

2. EXPERIMENTAL DETAILS

2.1 ALD viscous flow reactor

The WS_2 coatings were grown by sequential reaction of gas precursors WF_6 and H_2S at a temperature range of 250 to 350°C in a hot-wall viscous flow ALD reactor using N_2 as the carrier and purge gas. The reactor design shown in Fig. 1 was taken from the ALD viscous flow reactor of Elam et al [25]. The WF_6 and H_2S precursors were injected into the carrier gas stream using pneumatically operated valves. Their pulse times were 2 s and their purge times were 5 and 25 s for WF_6 and H_2S, respectively, at a total pressure of 2 Torr. Nitrogen gas was supplied via a

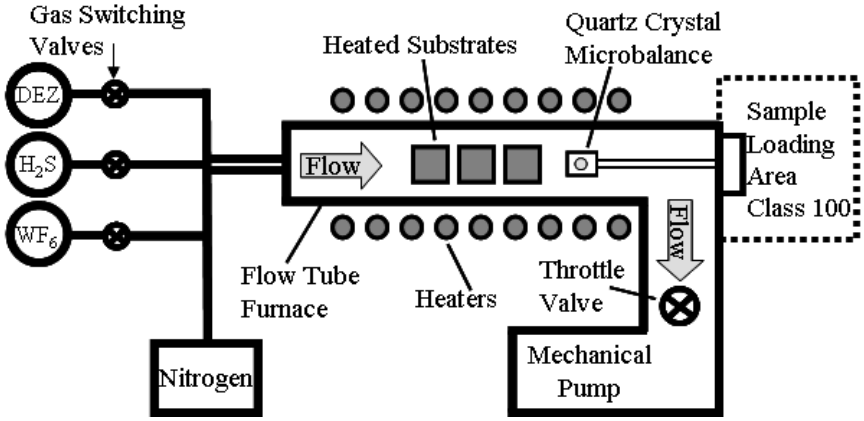

Fig. 1. Schematic of viscous flow reactor used to grow ALD coatings [after 25].

mass flow controller (MFC) with a throughput of 50 sccm on the reactant lines. A dry pump was used to reach a base pressure of approximately 5 mTorr. In order to measure growth rates, an *in situ* quartz crystal microbalance (QCM) stage was placed inside the stainless steel tube furnace. Prior to deposition, the substrates were ultrasonically cleaned in acetone, isopropyl alcohol, DI water, and then UV ozone cleaned for 20 minutes.

In order to commence the nucleation and growth of WS_2 by ALD, diethyl zinc $[(C_2H_5)_2Zn]$ catalytic liquid precursor was used to promote the adsorption and surface reaction of the WF_6 gas precursor, as we determined previously in [14,26]. Two different ALD recipes, referred to throughout the remainder of this paper, were utilized to deposit WS_2. The first recipe (recipe A) used a single diethyl zinc (DEZ) pulse followed by 50 cycles of WF_6 and H_2S [14]. This sequence was repeated 4 more times for a total of 5 sequences. The second recipe (recipe B) created one monolayer of ZnS using one pulse of DEZ and one pulse of H_2S [14,26]. This ZnS catalytic layer was then exposed to WF_6 and H_2S gas precursors to grow ALD WS_2. Successful WS_2 films using this recipe were grown up to 1500 WF_6 and H_2S ALD cycles. Depending on which recipe was used and the number of ALD WS_2 cycles, the total coating thickness ranged from ~ 10 to 30 nm on SiO_2 substrate to ~ 100 to 400 nm on 440C stainless steel and gold substrates, respectively.

2.2 Material characterization

Films were characterized by x-ray diffraction (XRD); dual focused ion beam (FIB) high resolution scanning electron microscopy (HRSEM); cross-sectional transmission electron microscopy (XTEM) with energy-dispersive x-ray spectrometry (EDXS) and selected area electron diffraction (SAED); and Auger electron spectroscopy (AES). Site-specific TEM specimens were prepared with a FEI DB-235 dual-beam FIB/HRSEM, and then analyzed in a FEI Tecnai F30-ST TEM/STEM operated at 300kV and equipped with EDXS. X-ray spectral images, where an entire spectrum is acquired from each point in a 2D array, were collected from both the wear surface and the unworn surface of specimens. Sandia's Automated eXpert Spectral Image Analysis (AXSIA) software was then used to analyze the data [27]. AXSIA quickly reduces large raw spectral images into a compact solution consisting of a small number of linearly independent component image/spectrum pairs. For display purposes the component images are often combined into an RGB color overlay. The AES sputter depth profiles were obtained using a Physical Electronics PHI680 Scanning Auger system. A 10 keV accelerating voltage and 25 nA beam current were used for data acquisition. Sputtering was performed using a rastered 2 keV argon ion beam. The sputter rate was determined to be 11 nm/min on a thermal SiO_2 film of known thickness.

2.3 Friction and Wear Testing

Friction measurements were made on planar surfaces using a ball-on-disk linear wear tester. The tests were performed in unidirectional sliding mode. The tester was housed in an environmental chamber. Oxygen content in the chamber was measured (Delta F Platinum Series oxygen monitor) and the dew point was monitored with a chilled mirror hygrometer. Tests were conducted in dry nitrogen (<10 ppm O_2 and <100 ppm H_2O) using a 3.175 mm diameter Si_3N_4 ball (Cerbec) with arithmetic surface roughness R_a of 3 nm, at normal loads of 98, 490, or 980 mN. These loads correspond to initial maximum Hertzian contact stresses (P_o) of ~ 0.3, 0.6 and 0.8 GPa, respectively. A 500 mN transducer (Sensotec) in the load arm measured the tangential load over a track distance of 1.6 mm. The sliding speed was 3.3 mm/s. The ratio of tangential to normal load is the friction coefficient. Friction and wear tests were run for either 1000 (short) or 50,000 (long) unidirectional cycles. The wear factor was calculated as the wear track volume divided by the load and by the total distance traveled by the ball. These wear track measurements were determined from a white light optical interferometer (Wyko NT1100 optical profiler).

2.4 Rolling Element Bearing Torque Testing

The fully assembled 440C stainless steel rolling element bearings (Timken Super Precision, part no. 3332FC) are shown in Fig. 2(a). The bearings had stamped stainless steel retainers, an outer race diameter of 4.74 mm, inner race diameter of 2.32 mm, and a 7 ball compliment. The bearings were loaded two per cartridge as shown in Fig. 2(b) for torque tests and vibration. Wavy washers and a locking end screw were used to adjust the bearings for a compressive axial preload of 10 lbf between the two bearings, which was determined by pressing on the central shaft with respect to the rectangular outer housing in an Instron servohydraulic load frame and observing the load-displacement curve. The cartridges were then installed in a torque testing device as shown in Fig. 2(c). In the configuration shown, the bearing torque is determined as the cartridge center shaft is rotated counter-clockwise while the outer rectangular housing is constrained by the load cell on one side and the adjustable post on the other side. In this manner, the bearings could be rotated through a small angular deflection during oscillation, and the position of the balls with respect to the races maintained as in the end-use application. The geometry of the bearing cartridge was determined to produce the same type of inertial response as the actual solenoid components during vibration testing.

Bearing torque was measured while rotating the center shaft of the cartridge counter-clockwise at 1 rev/min for a total of 2 revolutions. The force on the load cell was acquired at 10 Hz during this measurement, and multiplied by the lever arm (distance from shaft center line to

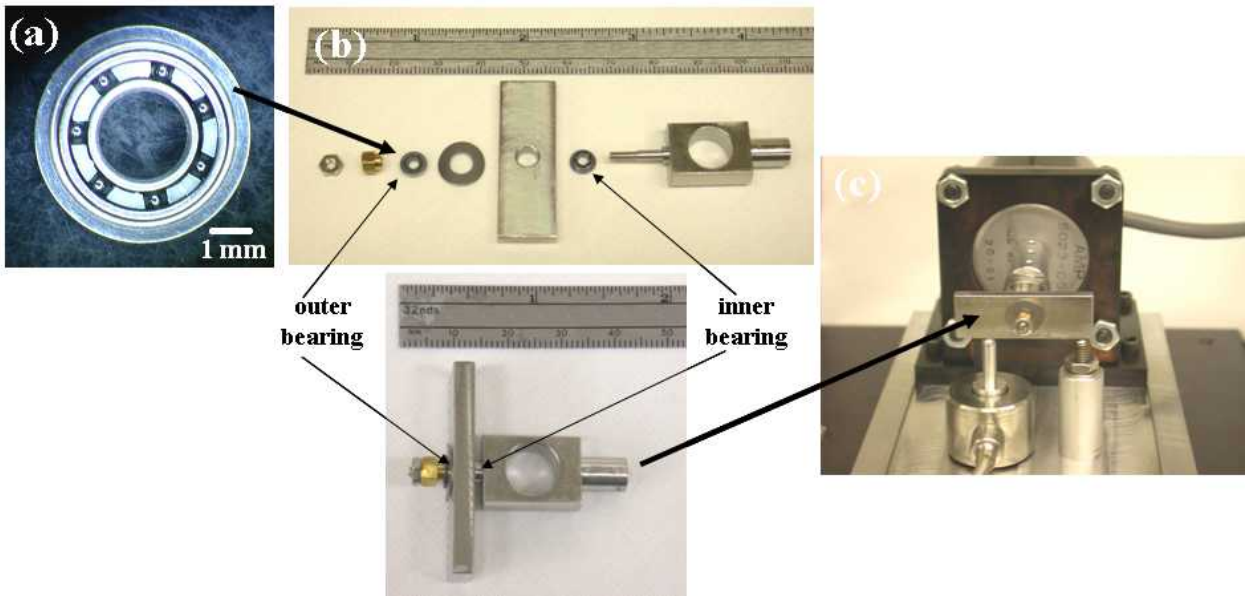

Fig. 2. Optical micrograph images of (a) individual 440C stainless steel rolling element bearing, (b) exploded view of bearing test cartridge assembly, and (c) bearing setup for torque measurements.

the point of load cell contact) to determine the torque. For analysis, the torque mean, noise (standard deviation), and maximum value were determined in the interval between 5% and 95% of these two full shaft rotations. In order to replicate the type of wear experienced in a candidate application, the bearing shaft was subjected to oscillations of +/- 30 degrees at an angular velocity equivalent to 200 rev/min.

The effects of vibration on bearing torque and lubricant performance were investigated by subjecting the bearings to vibration part-way through a sequence of oscillation and torque testing. The rectangular outer housing of the bearing cartridge was clamped rigidly to a plate in a vibration fixture, and the shaft portion was unconstrained. The fixture was subjected to 20 minutes of random vibration among two axes, radial and axial. The computed average level was 23.2 grams, with the spectral density shown in Table I.

Table I. Frequency Spectrum of Bearing Vibration Exposure

Frequency	**g^2/Hz**
10-30	0.015
80-450	1.05
1250-1900	.01
2000	.001

Bearing testing followed the following sequence:

- Perform initial torque measurement.
- Oscillate shaft a total of 18,000 cycles (+/- 30 degrees), stopping to measure bearing torque every 3600 oscillations.
- Perform bearing vibration exposure.
- Perform post-vibration torque measurement.
- Oscillate shaft an additional 54,000 cycles (for a total of 72,000 cycles), stopping to measure bearing torque every 9000 oscillations.

A number of different surface treatment approaches were evaluated in the bearing tests in addition to ALD WS_2. The surface treatments are shown in Table II.

Table II. Surface Treatments Investigated in Bearing Tests

Designation	Description
Unlubricated	Clean 440C balls and races.
Sputtered MoS_2	Nominally 1 mm thick sputtered MoS_2 doped with antimony oxide [28].
Impingement A	MoS_2 particles blasted at surface with inorganic binder (Microseal 200-1 [29]).
Impingement B	MoS_2 particles blasted at surface in a N_2 gas stream, no binder.
ALD WS_2, recipe A	One pulse of DEZ followed by 50 cycles of WF_6 and H_2S repeated 4 more times [14].
ALD WS_2, recipe B	One pulse of DEZ and one pulse of H_2S (=1 monolayer of ZnS) followed by up to 1500 cycles of WF_6 and H_2S [14,26].

In general, at least three cartridges containing bearings with the same surface treatment were tested, and the torque values averaged at each oscillation interval.

3. RESULTS AND DISCUSSION

3.1 Chemistry and growth

The WS_2 ALD is based on the CVD reaction:

$$WF_6\,(g) + 2H_2S\,(g) + H_2\,(g) \rightarrow WS_2\,(s) + 6HF\,(g) \qquad (1)$$

where WF_6 and H_2S are gas precursors one and two. Diethyl zinc (DEZ) liquid precursor was used as a reaction initiator, since we previously determined DEZ was a good reducing agent for WF_6 [14,26].

To study the WS_2 nucleation and growth processes in detail, *in situ* QCM measurements were performed using DEZ as a catalytic precursor. *In situ* QCM measurement shown in Fig. 3(a) indicated that WS_2 did not grow on the quartz crystal or any substrate material from 250 to 350ºC without the presence of a ZnS catalytic layer [26]. Also, the measured ALD growth of WS_2 was not constant, but slowed with number of ALD cycles. However, even 1 cycle of ZnS growth shown in Fig. 3(a) was adequate to restore high WS_2 growth rate (~ 1.1 Å/cycle) when its growth began to slow down.

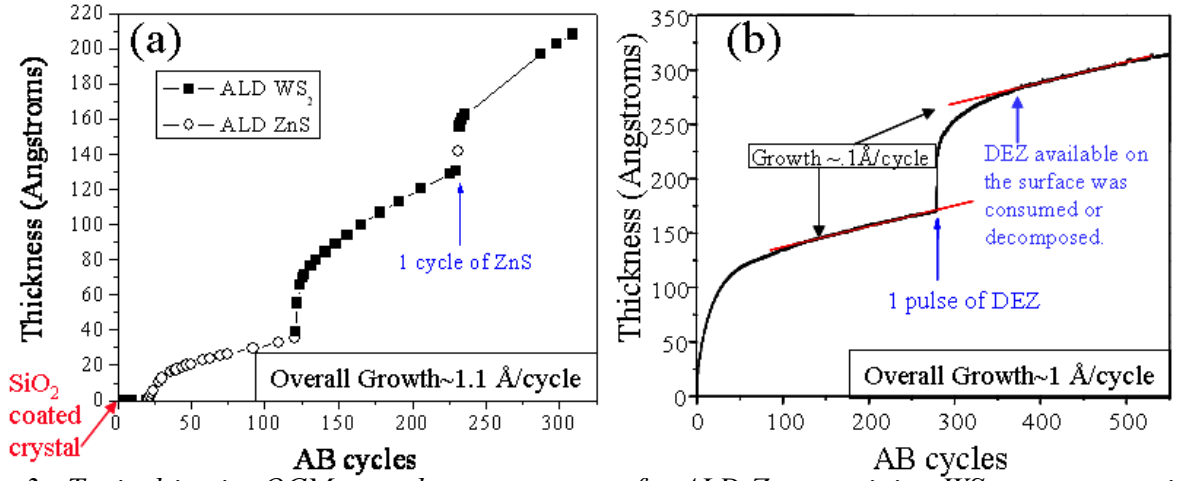

Fig. 3. Typical in situ QCM growth measurements for ALD Zn-containing WS_2 nanocomposites using (a) Recipe B [26]: 1 cycle of ZnS (1st-DEZ, 2nd-H_2S) then X number of WS_2 cycles (X=25, 100, 200, 400, 900, 1500), and (b) Recipe A [14]: 1 pulse of DEZ then 50 cycles of WS_2 (1st-WF_6, 2nd-H_2S) repeated 5 times.

Fig. 3(b) shows a typical *in situ* QCM measurement of the affects of the DEZ catalyst alone on the WS_2 chemistry [14]. Similar to the ZnS catalytic layer, one pulse is sufficient to restore high WS_2 growth rates. The *in situ* QCM measurements in Fig. 3(b) show the growth slows down, after an initial high growth region, to ~ 0.1 Å/cycle, likely when the DEZ available on the surface was consumed or decomposed. Since the *in situ* QCM measurements showed that the growth dropped off after 50 cycles, four subsequent 1 pulse DEZ and 50 cycles WS_2 sequences were repeated (recipe A). The overall growth rate, using low and high growth regions, was ~ 1.0 Å/cycle. This is a typical rate for ALD processes; however, most ALD reactions by definition follow a linear growth rate [22,23]. Since too much DEZ catalyst, 5 total sequences, resulted in excess zinc compounds and severe etching of the underlying substrates [14], a second recipe (recipe B) with less zinc precursor was used based on the original *in situ* QCM results in Fig. 3(a). In addition, the overall Zn-catalyzed WS_2 growth was found to vary dramatically between ~1 and 12 Å/ALD cycle depending on the free electron availability of the substrate, which has also been reported for CVD tungsten growth [30]. The higher growth per cycle was on conducting substrates such as gold which provides more free electrons at the surface compared to insulating substrates like SiO_2.

3.2 Microstructure

X-ray diffraction measurements for recipe A WS_2 coatings on insulating SiO_2 are shown in Fig. 4(a). XRD confirmed that the ~30 nm thick coatings grown at 300 and 350ºC were crystalline with predominantly hexagonal (002) texture. Basal planes with c-axis orientated parallel to the substrate surface [(100) and (101) reflections] are also shown at 350ºC, while at 300ºC the basal planes are primarily with c-axis orientated perpendicular to the substrate [(002) reflection], typical of metal dichalcogenide coating growth at high temperatures [18-21]. Fig. 4(b) shows corresponding plane-view HRSEM images of the WS_2 coatings illustrating the basal in-plane orientation differences with just 50ºC change in processing temperature. The crystallites of perpendicular-orientated basal planes have approximate growth dimensions of 50 to 100 nm, while those in the parallel-orientated coatings have growth dimensions of approximately 40 to 70 nm. The edge islands are anisotropic since the width along the <002> basal plane direction is less than the length along the edge plane <100> or <101> directions, inferred from the crystallite length being less than the film thickness. Furthermore, the perpendicular orientated basal planes in Fig. 4(b) appear to be growing above and shadowing the adjacent parallel orientated basal planes, similar to sputter deposited MoS_2 coatings [31].

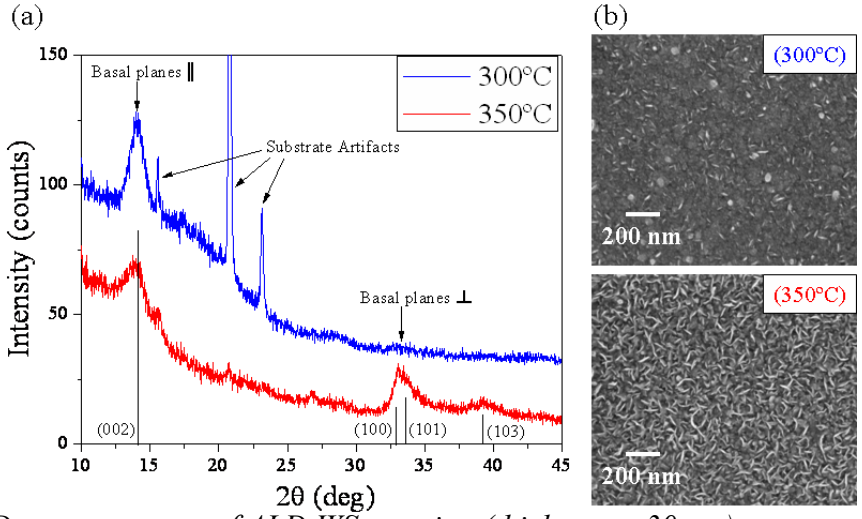

Fig. 4. (a) XRD measurements of ALD WS_2 coating (thickness ~ 30 nm) grown on silicon at 300 and 350ºC. (b) Corresponding HRSEM images of the coatings at 300 and 350ºC showing predominantly curved basal planes orientated perpendicular to substrate with increasing process temperature.

Fig. 5 shows (a) AXSIA and (b) XTEM images, and (c) Auger depth profile for an ~393 nm thick WS_2 coating (recipe B) on gold [14]. AXSIA analysis confirms nanometer sized ZnF_2 is present through the coating thickness, since it is a product of the zinc reduction of WF_6 in the growth process. AXSIA also shows the WS_2 constituents are present throughout the thickness of the coating. No ZnS was found in the coating, since ZnS was likely consumed or decomposed as the coating thickness increased. In addition, Fig. 6(b) shows strongly textured crystalline WS_2 basal planes throughout the thickness of the coating (see arrows). The 2H-WS_2 randomly orientated basal planes are evident along with a small amount of ZnF_2 clusters, whose presence is supported by the low atomic concentration of Zn and F in the Auger depth profile in Fig. 6(c). Note that stoichiometric composition ratios of W, S, Zn, and F could not be made due to preferential sputtering of the coating during depth profiles. It was further determined from a selected area electron diffraction (SAED) pattern of the randomly orientated basal planes that the WS_2 interlamellar d-spacing for (002) was ~ 6.4Å in good agreement with indexed (PDF#03-065-7515) 6.2Å lattice spacing in the c-direction.

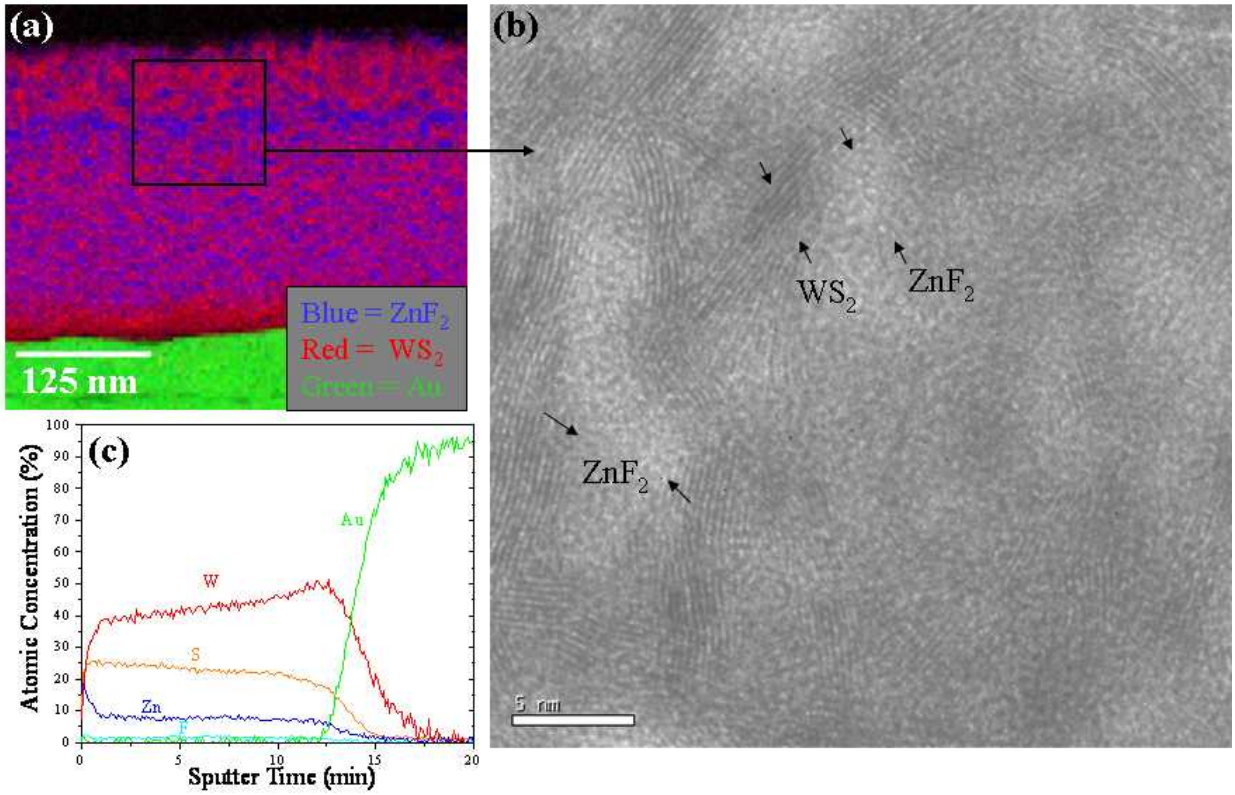

Fig. 6. (a) Cross-sectional x-ray spectral imaging map of 393 nm thick coating (900 WS_2 cycles) taken from (b) HRTEM image. Corresponding elemental EDS spectra are shown as pixels in green=Au, blue=ZnF_2, and red=WS_2. Arrows in (b) indicate WS_2 basal planes and likely ZnF_2 clusters. (c) Representative Auger depth profile is shown through the coating into the substrate.

3.3 Tribology

The plot in Fig. 6 shows coefficients of friction (COF), μ, as a function of unidirectional sliding cycle for recipe A WS_2 (Fig. 3(b)) coatings [14]. The WS_2 coatings grown to ~120 nm thickness on 440C stainless steel and ~30 nm thickness on SiO_2 substrates exhibit extremely low COF, ~ 0.008 to 0.024, compared to the same respective substrates without the coating (COF from 0.6 to 0.8). The (002) basal planes orientated perpendicular to the substrate that form at 350ºC growth temperature, shown in Fig. 4, likely bend under shear loading and thus are re-orientated flat and transfer to the rubbing counterface assuring low friction at the high contact

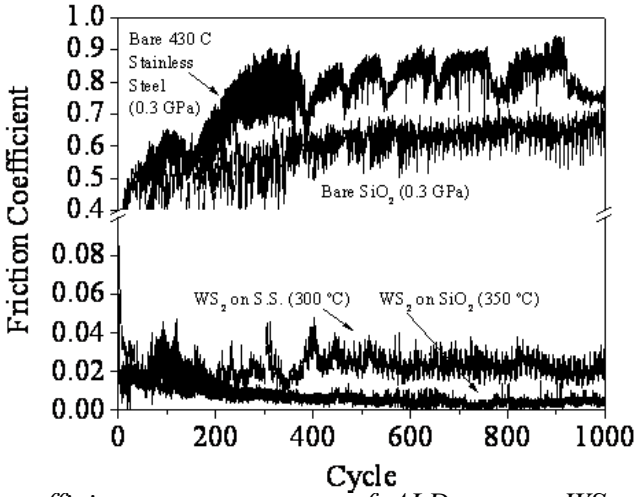

Fig. 6. Friction coefficient measurements of ALD grown WS_2 on stainless steel and SiO_2 substrates at varying contact stresses in dry nitrogen. Referenced friction coefficients of bare substrates are shown for comparison.

stresses [1-4,11-13,31].

One of the drawbacks for any solid lubricant coating is that due to lack of replenishment, it will eventually wear out (coating and/or transfer film) depending on the environment, loading conditions, coating thickness, and ability of the contact geometry to trap debris. We recently determined the thicker, lower zinc WS_2 nanocomposite coatings deposited using recipe B in Fig. 3(a) exhibited very low steady-state friction coefficients, ~0.09, 0.01, 0.008, for three Hertzian contact stresses of 0.3, 0.5, 0.6 GPa, respectively, to 50,000 cycles [14]. The coatings also exhibited very long wear life with no evidence of delamination or being worn out, since there were no excursions in the friction coefficients. The wear factors for the coating after 50,000 cycles from low to high contact stress are 2.4×10^{-7}, 6.5×10^{-7}, and 4.3×10^{-7} $mm^3/N \cdot m$, respectively, which compare well to other solid lubricant coatings (MoS_2 [4] and DLN [32]) in dry environments.

3.4 Rolling Element Bearing Torque Testing

Fig. 7 shows average torque as a function of oscillation cycles for a variety of lubricants from Table II in lab air (~20% RH). The plot shows the unlubricated bearings exhibit high torque and noise due to adhesive wear of balls and races. The ALD WS_2 coating did not perform as well as the thicker MoS_2 coated bearings (sputtered and impingement coatings), which all meet the application torque requirement of < 3 mN.m.

Due to the greater amount of Zn-containing compounds (more DEZ-catalyst) in these coatings associated with recipe A, bearings were treated with recipe B in an attempt to lower the bearing torque values. Five bearing test cartridges (ALD_6 to ALD_10) with thicknesses of ~80 nm were created and tested according to the following conditions:

Cartridge	Deposition Temp.(ºC)	WS_2 cycles	Test Environment
ALD_6	300	900	lab air
ALD_7	300	900	dry N_2
ALD_8	250	1500	lab air
ALD_9	250	1500	dry N_2
ALD_10	250	1500	lab air

Fig. 8 shows the torque results for these tests. ALD coatings exhibited large torque values for tests in ~20% RH lab air, thus they do not meet performance requirements in this

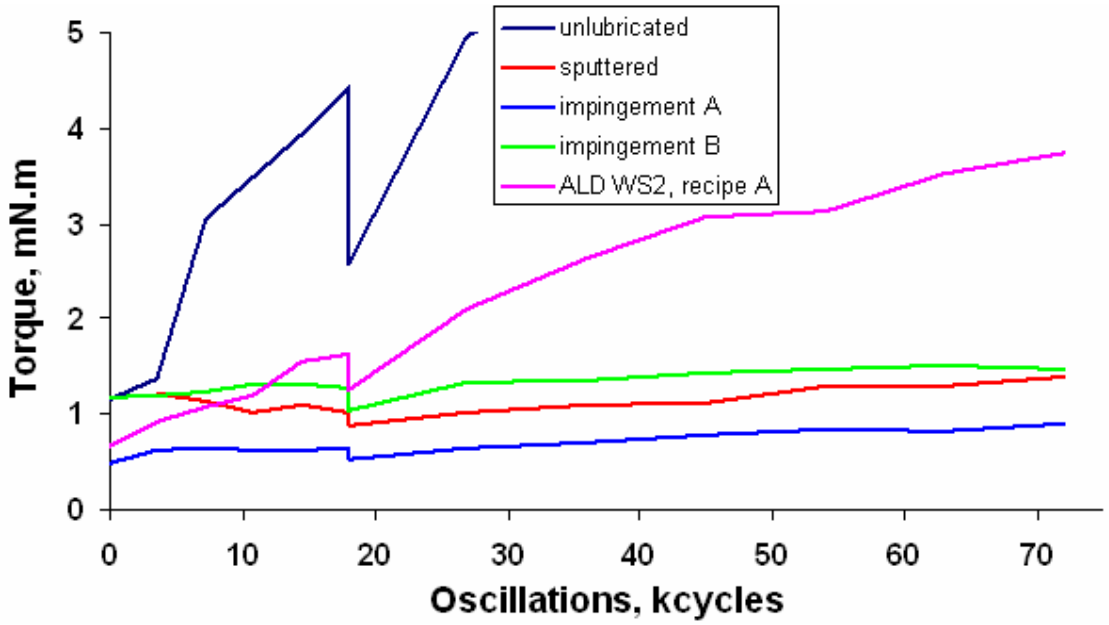

Fig. 7. Average torque of several solid lubricant coatings(Table I) out to 72000 oscillations tested in lab air (~20 %RH).

environment. On the other hand, the ALD coatings exhibited torque values consistently less than 1.5 mN.m in dry N_2, except for one measurement of 6 mN.m at 63 kcycles, which may be attributable to a particle getting into the race temporarily or cage binding, as it recovered low torque during the next measurement interval. This performance is comparable to that for impingement MoS_2 coatings shown in Fig. 7.

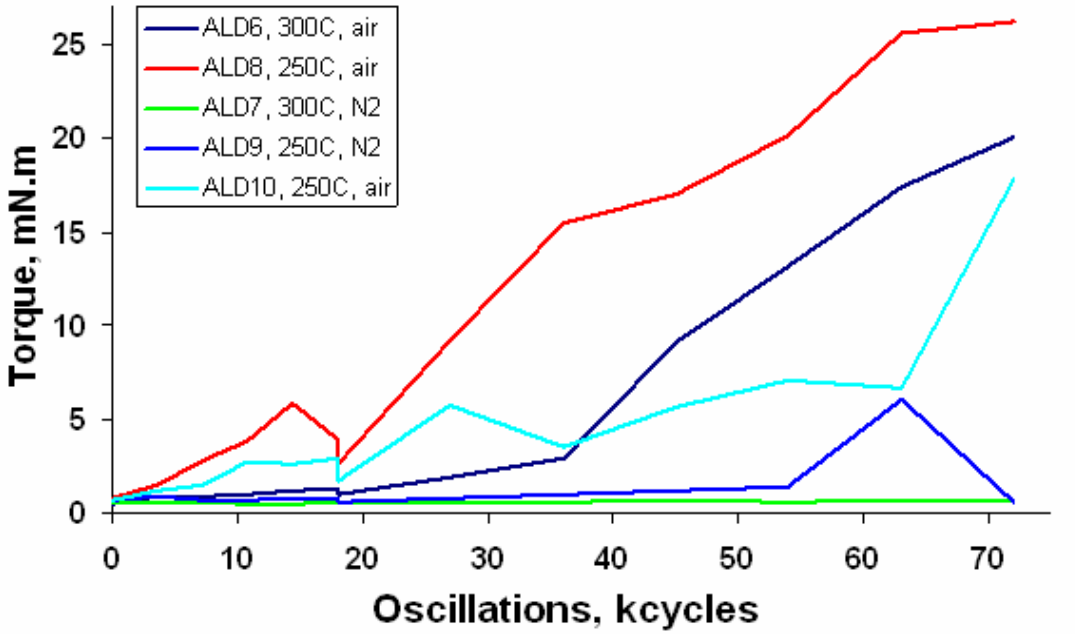

Fig. 8. Average torque behavior of ALD WS_2 solid lubricant coatings grown at 250 and 300ºC to 72000 oscillations under lab air (~20 %RH) and dry nitrogen testing environments.

3.5 HRSEM and EDS of Disassembled ALD WS_2 Coated Rolling Element Bearings after Torque Testing in Dry Nitrogen

Fig. 9 shows a sequence of HRSEM images of the disassembled bearing inner race for ALD_7 (300ºC in dry N_2) test cartridge after 72000 oscillations. The whole inner race area is shown in Fig. 9(a). Fig. 9(b) shows a higher magnification image of the heavily loaded side

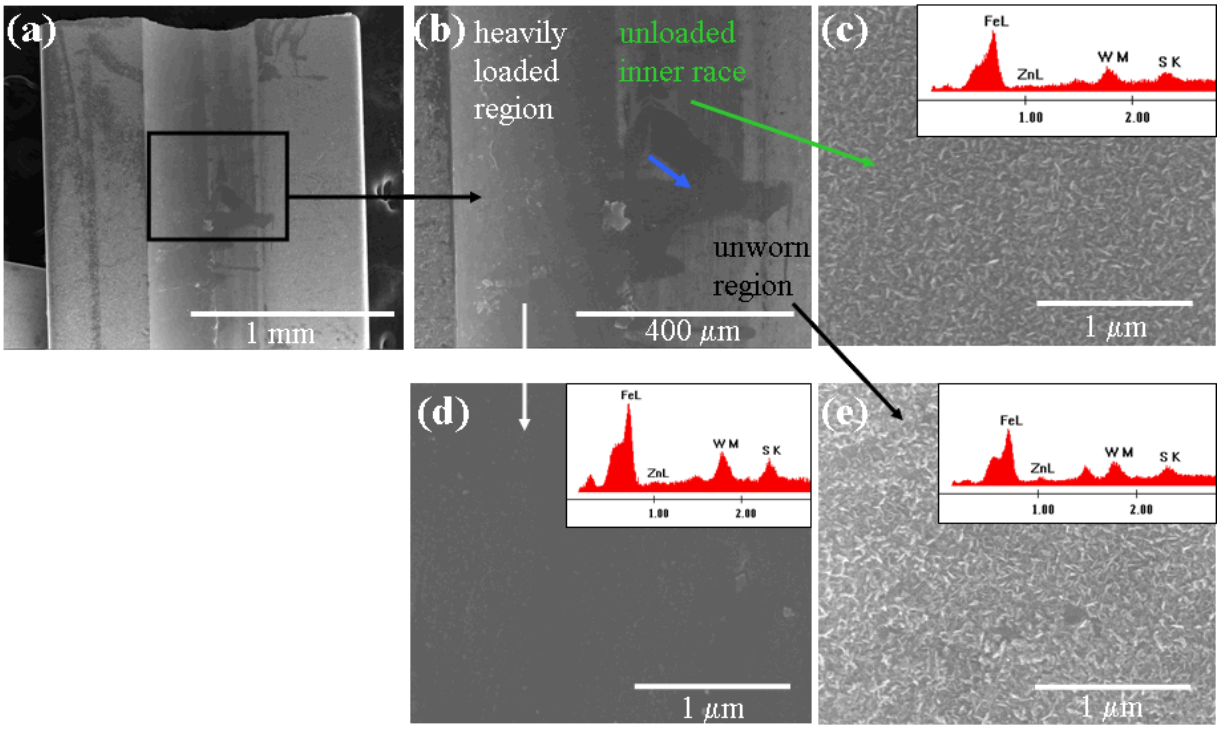

Fig. 9. HRSEM images and corresponding EDS of inner race of ALD WS_2 lubricated bearing (grown at 300ºC, tested in dry nitrogen).

where the axially preloaded balls roll. Also shown in the inner race area is the unloaded side. The extraneous marking shown with the arrow in Fig. 9(b) is likely a result of the ball being allowed to contact this portion when the bearing was dissembled, since the remainder of this area shown in Fig. 9(a) is untouched. Fig. 9(c) shows a higher magnification image of the unloaded inner race area. The microstructure is similar to Fig. 4(b) showing ALD WS_2 basal planes with c-axis orientated parallel to the substrate surface. However, in this case this texture was evident at 300ºC, while in Fig. 4(b) this texture was observed at 350°C growth temperature, and not at 300°C. The difference in growth texture at the same processing temperature is likely due to differences in substrate nucleation and growth, i.e. on silicon versus stainless steel. In addition, ALD was successful in conformally coating the entire inner race. Fig. 9(d) shows a higher magnification image of the heavily loaded inner race area where the ball bearings experience rolling, oscillation, and vibration. It is evident from Fig. 9(d) that the WS_2 basal planes have undergone compaction during the rolling process. In addition, there is some evidence of third body debris, possibly transfer film buildup. Accompanying EDS spectra are also shown for these images. The unworn or untouched area shows ALD coating constituents W, S, and Zn (from the catalyst) x-ray lines. Fe is observed from the underlying stainless steel due to the coatings being very thin. The EDS spectrum from the heavily loaded, compacted region also shows that coating constituents are still present after 72000 oscillations.

Fig. 10 shows the accompanying HRSEM images of the disassembled bearing (a) outer race, and (e) a ball bearing for ALD_7 (300ºC in dry N_2) test cartridge after 72000 oscillations. Similar to the inner race, there is a heavily axially loaded side and unloaded side in the ball groove of the outer race, Fig. 10(b). Fig. 10(c) shows a higher magnification image of the WS_2 compaction and third body debris or transfer film buildup during this rolling process. Fig. 10(d)

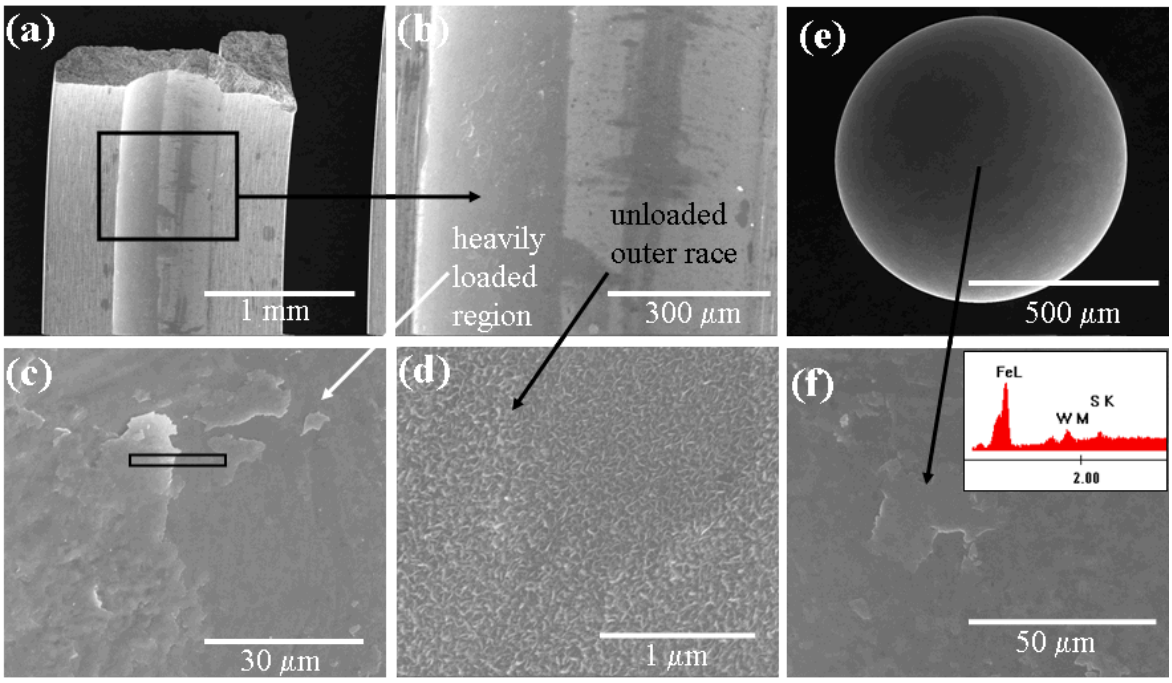

Fig. 10. HRSEM images and corresponding EDS of disassembled rolling element bearing (a) outer race and (e) a ball bearing of ALD WS_2 solid lubricant coatings grown at 300°C to 72000 oscillations in dry nitrogen testing environment. Box in (c) shows location of FIB-cut shown in Fig. 11.

again shows WS_2 basal plane orientation in unloaded region. Fig. 10(f) is a higher magnification image of one of the seven ball bearing surfaces. Similar to the loaded outer and inner races there is wear debris or transfer film present on the surface. EDS of the steel ball showed W and S x-ray lines present.

In order to elucidate the structure of the third bodies (wear debris or transfer film buildup) shown in Fig. 10(c), a FIB-cut was performed on the surface of the outer race located by the box in Fig. 10(c). Fig. 11 shows this FIB-cut through the third bodies. The higher magnification image shows the ~80 nm thick ALD WS_2 film under the wear debris or transfer film layer is still present after 72000 oscillations. The structure of the third body layer exhibits a "scalloping" appearance which is not an artifact of the FIB-cut process. This layering may be buildup of transfer film or wear fragments, although XTEM and chemical profiling are needed to confirm which one. The presence of the coating with associated third bodies and lack of tribo-oxidation are likely responsible for the observed low torque values in dry nitrogen.

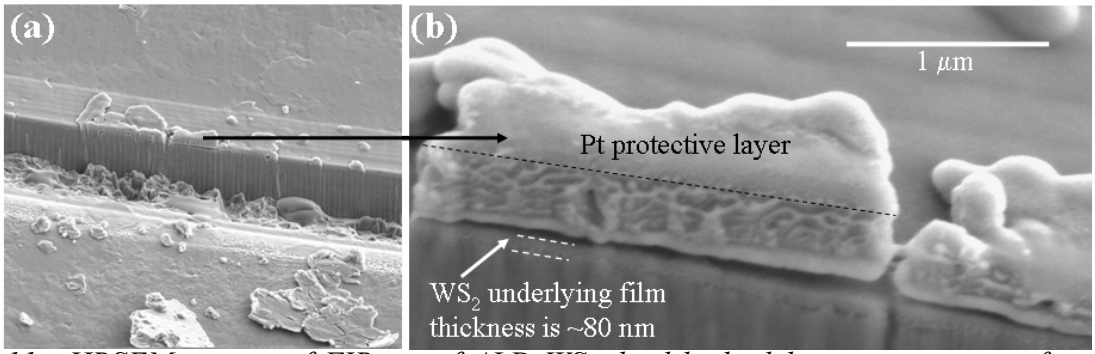

Fig. 11. HRSEM images of FIB-cut of ALD WS_2 third body debris on outer race from image location shown in Fig. 10(c). Pt layer was put down to protect the structure of the surface layers.

The bearings tested at 250ºC were not looked at since they had similar torque behavior. In addition, the issue of tempering, i.e. softening due to grain growth, of the 440C stainless steel at higher growth temperatures was not an issue with the torque behavior because the values were approximately the same at 300ºC compared to 250ºC, shown in Fig. 10. At even higher ALD growth temperatures, a slight drop in Rockwell C hardness was exhibited for ALD WS_2 on 440C stainless steel coupons, i.e. 59 to 55 from 350ºC to 300ºC, respectively. Although somewhat tempered, this would be less of an issue for decreased temperatures of 250 and 300ºC used here.

3.6 HRSEM and EDS of Disassembled ALD WS_2 Coated Rolling Element Bearings after Torque Testing in Lab Air

Fig. 12 shows a sequence of HRSEM images of the disassembled bearing inner race for ALD_6 (300ºC in lab air, ~20% RH) test cartridge after 72000 oscillations. Fig. 12(a) shows an image of the heavily loaded side, where the axially preloaded balls roll, as well as the unloaded side. WS_2 basal planes perpendicular to the stainless steel surface were observed in the unloaded and unworn regions, similar to Fig. 9(c). In contrast, inside the heavily loaded region (Fig. 12(b)), the inner race exhibited almost total oxidation of the ALD WS_2 coating. EDS confirmed that there were oxidized particles and some areas with no coating, i.e. bare steel.

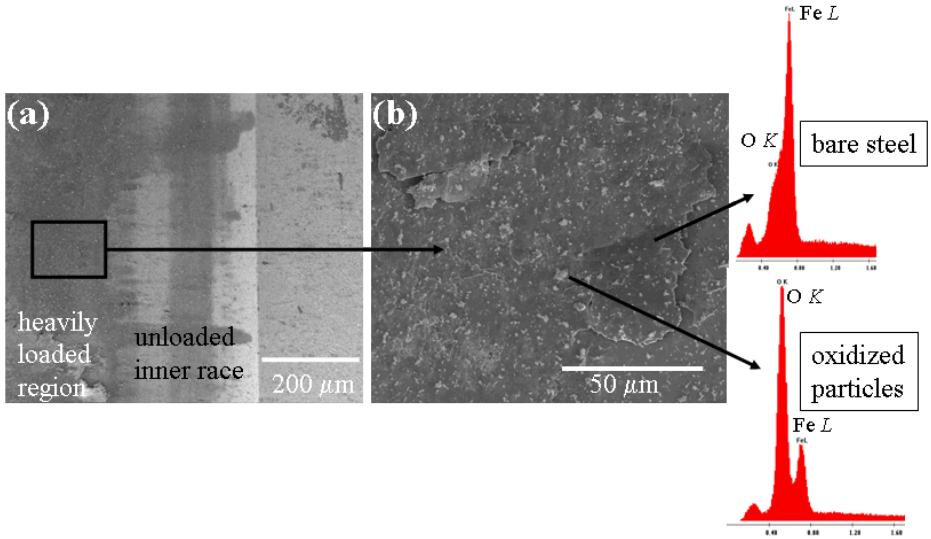

Fig. 12. HRSEM images and corresponding EDS of disassembled rolling element bearing inner race of ALD WS_2 solid lubricant coatings grown at 300ºC out to 72000 oscillations in lab air testing environment.

In addition, Fig. 12(b) shows evidence of cracks, which may be subsurface fatigue cracks that nucleated in the stainless steel and propagated to the surface. A FIB-cut at this location is needed to confirm rolling contact fatigue with subsequent cracking, since usually rolling element contact fatigue is witnessed after millions of cycles. However, the torque testing to 72,000 oscillations may have accelerated this process.

Fig. 13(a) displays the accompanying HRSEM images of the disassembled bearing outer race for ALD_6 (300ºC in lab air) test cartridge after 72000 oscillations. Fig. 13(b) shows a higher magnification image of the heavily axially loaded side with similar morphology to the inner race shown in Fig. 12(b). EDS of this area shows more oxidation compared to dry nitrogen testing along with some remaining WS_2 coating. A FIB-cut, whose location is shown in Fig. 13(b), was made inside the heavily loaded region to determine the structure and constituents of the surface and subsurface. Figs. 13(c)-13(e) show a three region transient zone of oxidized wear debris on top of the WS_2 coating, WS_2 (thinned) coating only, and bare steel, respectively. In contrast to the dry nitrogen test, this bearing cartridge did not exhibit uniform WS_2

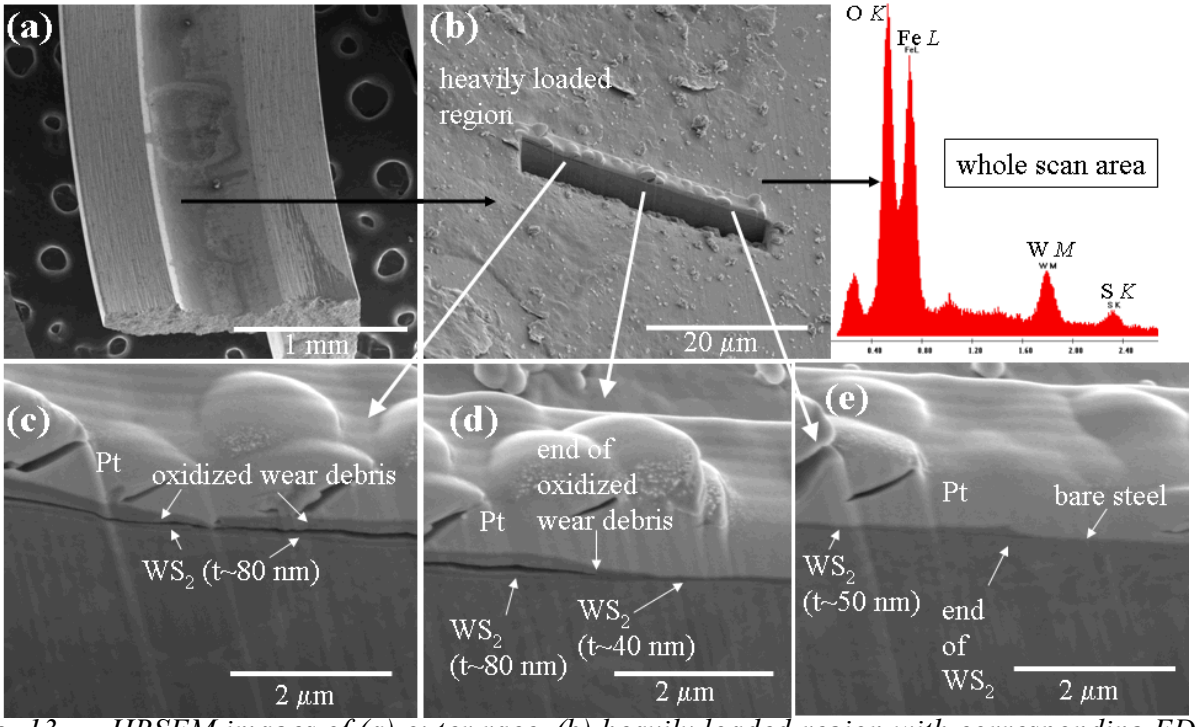

Fig. 13. . HRSEM images of (a) outer race, (b) heavily loaded region with corresponding EDS spectrum, (c)-(e) FIB-cut of ALD WS_2 coating grown at 300ºC to 72000 oscillations in lab air testing environment. A Pt layer was put down to protect the structure of the surface layers.

compaction and third body debris/transfer film buildup. The latter, previously shown in Fig. 11 (b), was not evident inside the races for lab air testing. XTEM and chemical profiling are needed to confirm this analysis.

Fig. 14 shows HRSEM images of one of the seven ball bearing surfaces after testing in lab air. In contrast to the balls tested in dry nitrogen, there is total oxidation (large amount of oxidized wear debris) and no WS2 coating remaining on the ball.

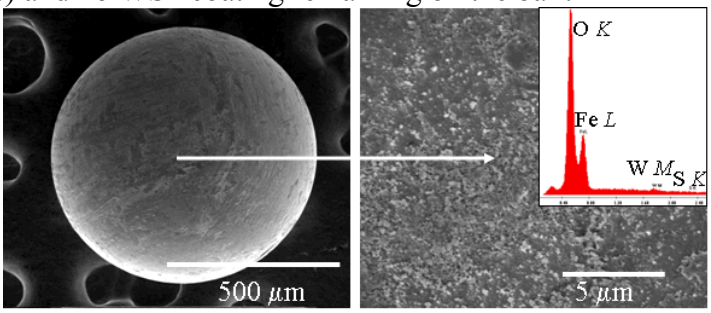

Fig. 14. HRSEM images and EDS spectrum of ball bearing surface after testing in lab air.

4. CONCLUSIONS

The interrelationships between layer growth, microstructure, tribological (rolling and sliding) behavior of ALD Zn-containing WS_2 nanocomposite coatings have been studied for rolling element bearing applications requiring friction, wear, and torque mitigation. The conformal and uniform coatings exhibited very low friction (μ~0.008) and wear factors (2.4×10^{-7} $mm^3/N \cdot m$) in pure sliding contact. Torque values in dry nitrogen on miniature stainless steel rolling element bearings were below 1.5 mN.m, and the coating was deposited conformally inside the bearing without disassembly. The hexagonal crystal texture of ALD WS_2 is temperature dependent. Shear-induced reorientation of the basal planes at high contact stresses

assured low friction and torque in dry nitrogen regardless of the as-deposited microstructure and orientation. For fully assembled rolling element bearing tests the outer race, inner race and ball surfaces showed evidence of third body, possibly transfer film, protection necessary to achieve low torque in dry nitrogen. In contrast, testing in air produced almost total oxidation and wear of the WS_2 coatings, and some areas with no WS_2. The ALD deposition of solid lubricants for miniature bearings is thus an attractive alternative to present lubrication methods since it offers the potential for reduced particulate contamination, more consistent run-in behavior due to more uniform lubricant distribution, and the ability to use relatively low cost, fully-assembled stainless steel bearings and batch processing to minimize lubrication process costs.

Acknowledgments
We appreciate technical assistance from M.J. Rye, P.G. Kotula, B.B. McKenzie, R.W. Buttry, R. Tissot, Liz Huffman, and R.D. Garfield. Sandia National Laboratories is a multiprogram laboratory operated by Sandia Corp., a Lockheed Martin Company, for the U.S. Department of Energy under Contract No. DE-AC04-94AL85000.

REFERENCES

1. Spalvins T J. Vac. Sci. Tech. 1987; A5:212.
2. Didziulis SV, Fleischauer PD, Soriano BL, Gardos MN Surface Coat. Technol. 1990; 43-44: 652.
3. Prasad SV, Zabinski JS Nature 1997; 387: 761.
4. Singer IL, Fundamental in Friction: Macroscopic and Microscopic Processes: Kluwer, Academic, Dordrecht, Netherlands; 1992 p. 237.
5. Singer IL, Bolster RN, Wegand J, Fayeulle S., Stupp BC Appl. Phys. Lett. 1990; 57: 995.
6. Wahl KJ, Belin M, Singer IL Wear 1998; 214: 212.
7. Donnet C, Erdemir A Trib. Lett. 2004; 17: 389.
8. Brainard WA, NASA TN D5141 1969.
9. Sliney HE, Trib. Int. 1992; 15: 303.
10. Prasad SV, McDevitt NT, Zabinski JS Wear 2000; 237: 186.
11. Martin JM, Donnet C, LeMogne Th, Epicier Th Phys. Rev. B 1993; 48: 10583.
12. Lince JR, Hilton MR, Bommannavar AS Surf. Coat. Tech. 1990; 43-44: 640.
13. Prasad SV, Zabinski JS, McDevitt NT Trib. Trans. 1995; 38: 57.
14. Scharf TW, Prasad SV, Dugger MT, Kotula PG, Goeke RS, Grubbs RK accepted Acta. Mater. 2006.
15. Moser J, Levy F J. Mater. Res. 1993; 8: 206.
16. Donley MS, McDevitt NT, Haas TW, Murray PT, Grant JT Thin Solid Films 1989; 168: 335.
17. Gardos, MN Trib. Lett 1995; 1: 67.
18. Lee WY, Besmann TM, Stott MW J. Mater. Res. 1994; 9: 1474.
19. Lee WY, More KL J. Mater. Res. 1995; 10: 49.
20. Cheon J, Gozum JE, Girolami GS Chem. Mater. 1997; 9: 1847.
21. Chung JW, Dai ZR, Ohuchi FS J. of Crystal Growth 1998; 186: 137.
22. Suntola T, Hyvärinen J Annu. Rev. Mater. Sci. 1985; 15: 177.
23. Ritala M., Leskela M, in Handbook of Thin Films: edited by H.S. Nalwa, Academic, San Diego 2002; 1: 103.
24. George SM, Ott AW, Klaus JW J. Phys. Chem. 1996; 100: 13121.
25. Elam JW, Groner MD, George SD Rev. Sci. Instrum. 2002; 73: 2981.
26. Scharf TW, Prasad SV, Mayer TM, Goeke RS, Dugger MT J. Mater. Res. 2004; 19: 3443.
27. Kotula PG, Keenan MR, Michael JR Microsc. Microanal. 2003; 9: 1.
28. http://www.hohmanplating.com
29. http://www.em-corporation.com
30. Chang KM, Wang SW, Li CH, Tsai JY, Yeh TH Jpn. J. Appl. Phys. 1996; 35: 6555.
31. Hilton MR, Jayaram G, Marks LD J. Mater. Res. 1998; 13: 1022.
32. Scharf TW, Singer IL Trib. Trans. 2002; 45: 363.